Environ. Sci. Technol. **2005**, *39,* 1324−1331

Actinide Sequestration Using Self-Assembled Monolayers on Mesoporous Supports

GLEN E. FRYXELL,* YUEHE LIN, SANDY FISKUM, JEROME C. BIRNBAUM, AND HONG WU

Materials Synthesis & Modification Group, Pacific Northwest National Laboratory, P.O. Box 999, Mailstop K2-44, Richland, Washington 99352

KEN KEMNER AND SHELLEY KELLY

Argonne National Laboratory, 9700 South Cass Avenue, Argonne, Illinois 60439

Surfactant templated synthesis of mesoporous ceramics provides a versatile foundation upon which to create high efficiency environmental sorbents. These nanoporous ceramic oxides condense a huge amount of surface area into a very small volume. The ceramic oxide interface is receptive to surface functionalization through molecular self-assembly. The marriage of mesoporous ceramics with self-assembled monolayer chemistry creates a powerful new class of environmental sorbent materials called self-assembled monolayers on mesoporous supports (SAMMS). These SAMMS materials are highly efficient sorbents whose interfacial chemistry can be fine-tuned to selectively sequester a specific target species, such as heavy metals, tetrahedral oxometalate anions, and radionuclides. Details addressing the design, synthesis, and characterization of SAMMS materials specifically designed to sequester actinides, of central importance to the environmental cleanup necessary after 40 years of weapons-grade plutonium production, as well as evaluation of their binding affinities and kinetics are presented.

Introduction

Over the past decade, a great deal has been learned about making nanostructured materials. In recent years there has been a shift from asking "What shapes can be made?" to asking "What can these shapes be made to do?" This has required that the nanostructured materials be inherently *functional*. One of the areas that shows great promise for these functional nanomaterials is their use in the field of environmental remediation. Recently, significant advances have been made in the synthesis of functional nanomaterials (*1*−*45*) creating exciting new possibilities for the sequestration of toxic materials from the environment.

The U.S. Department of Energy is faced with a daunting environmental cleanup resulting from 40 years of weapons-grade plutonium production. A central focus of this cleanup effort is the ability to selectively and completely remove the radionuclides from complex mixtures so that high-level waste (HLW) volume can be minimized and the nonradioactive components can be segregated and disposed of as low-level waste (LLW), thus substantially reducing the cost of the remediation process. In addition, the short-term risk assessment for tank closure requires a complete and accurate accounting of actinide speciation. This can be done either via direct separation or by concentration of low-level actinides and subsequent separation from the matrix. Isolation of individual actinides such as americium is a key parameter in the risk assessment necessary for tank closure. There are currently no methods available to distinguish or separate americium from plutonium at extremely low concentrations. This is essential information for the short-term risk assessment for HLW tank closure.

These needs dictate the development of selective and efficient separation of actinides from complex waste streams so as to minimize HLW volume, reduce waste management costs, and enhance long-term stability of the HLW form. Recently the U.S. DOE has placed emphasis on the need to significantly reduce the volume of material put through the vitrification process. Thus, selective separation of the actinides and radiocesium from tank waste forms a critical need for this waste cleanup strategy.

The area of functionalized nanoporous ceramics has received a great deal of attention in recent years (*1*−*28*). The field has been reviewed (*29*−*31*). We have developed self-assembled monolayers on mesoporous supports (SAMMS) as a superior method of mercury and heavy metal sequestration, proving to be orders of magnitude faster and more effective than existing mercury-scavenging methods (*32*−*38*) (see also refs *10*−*12*). This research was extended to include anions (*39*, *40*) (see also refs *41* and *42*), cesium (*43*), and radioiodine (*44*). This background provided the foundation for the current work, which extends the interfacial chemistry of monolayer-coated mesoporous ceramics to the sequestration of actinides.

The highly ordered nanostructure of SAMMS is the culmination of three successive generations of molecular self-assembly. The first generation is the aggregation of the surfactant molecules to create the micelle template; the second is the aggregation of the silicate coated micelles into the mesostructured greenbody, and the third is the self-assembly of the silane molecules into an ordered monolayer structure across the pore interface (see Figure 1). This functionalized hexagonal honeycomb structure is a powerful foundation upon which to build an environmental sorbent material.

The SAMMS concept allows for significant freedom in the design and synthesis of tailored materials for actinide separation. The mesoporous ceramic synthesis is quite general and can be used to prepare a variety of high surface area ceramic oxide supports that are stable in different environments (acidic, corrosive, oxidizing, etc.). The high surface area of the mesoporous support (ca. 1000 m^2/g) coupled with the high population density of binding groups creates a high loading capacity in the final SAMMS material. The rigid, open pore structure of the mesoporous support makes all of the interfacial binding sites available to solution-borne species and allows for facile diffusion into the porous matrix, resulting in rapid sorption kinetics. The chemical specificity of a given type of SAMMS is governed by the monolayer interface. The ability to install chemically different monolayers, along with the ability to synthetically elaborate those monolayers post-installation, allows for a wide variety of binding chemistries to be installed, making the SAMMS concept easily tailored for a variety of environmental targets (Pu, Cs, TcO_4, etc.). SAMMS, being a silica-based technology, would be readily incorporated into a vitrification process stream. This would reduce the volume of waste needing

* Corresponding author phone: (509)375-3856; fax: (509)375-2186; e-mail: glen.fryxell@pnl.gov.

10.1021/es049201j CCC: $30.25
Published on Web 01/12/2005

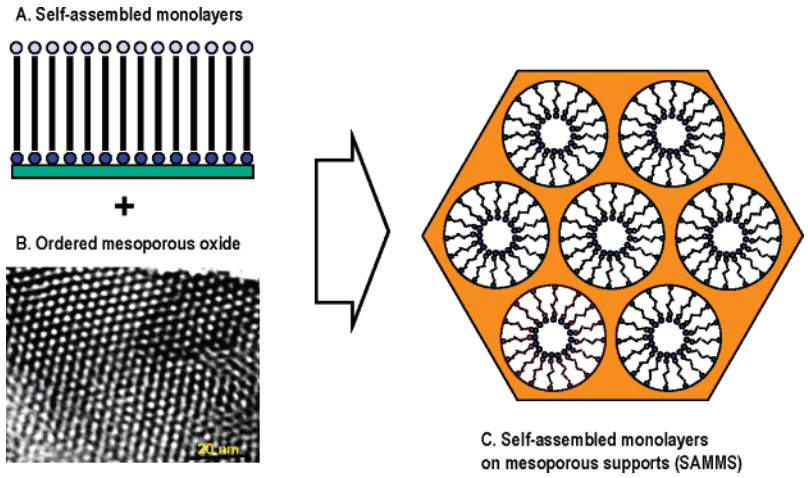

FIGURE 1. Genesis of SAMMS.

vitrification significantly since only the volume of the radionuclide-laden SAMMS would have to be vitrified and not the bulk of the waste. This paper summarizes some of our work in the design, synthesis, and performance evaluation of actinide-specific SAMMS.

Experimental Section

Materials. MCM-41 was prepared as described previously (*32*, *34*). 3-Aminopropyl trimethoxysilane and (2-aminoethyl)-3-aminopropyl trimethoxysilane were obtained from United Chemical Technologies. The acetamidephosphonate ("Ac-Phos") silane and propionamidephosphonate ("Prop-Phos") silane were prepared as described previously (*45*).

The self-assembled monolayers were deposited in MCM-41 (60−65 Å pores, 880−900 m^2/g) by carefully prehydrating the ceramic with approximately 2−2.5 monolayers worth of water (approximately 0.32 mL of water for each 1.0 g of MCM-41), followed by treatment with a slight (ca. 10−15%) excess of silane (relative to available surface area), and the mixture was held at toluene reflux for 4−6 h. The mixture was then cooled to ambient temperature and filtered, and the collected solid was washed copiously with 2-propanol. The SAMMS were then air-dried to constant weight in a fume hood and characterized using solid-state ^{29}Si and ^{13}C NMR, BET, and in some cases EXAFS and XPS.

The phosphonic ester was cleaved post-deposition using trimethylsilyl iodide (TMSI), either in anhydrous acetonitrile for 18 h at ambient temperature, or pure in the vapor phase at 80 °C, followed by aqueous hydrolysis for 1 h.

Measurements. (a) NMR. Solid-state ^{29}Si and ^{13}C NMR spectra were determined at 19.944 and 25.2458 MHz, respectively, using a Chemagnetics CMX-100 NMR quadruple channel spectrometer system. The probe was a 7-mm pencil-type probe with magic angle spinning at 4 kHz. The 4-μs 90-deg pulses were utilized for both ^{29}Si and ^{13}C, with proton decoupling power at 62.5 kHz.

^{29}Si spectra were acquired using the Freeman-Hill T1 (t1fh) pulse sequence with a short recovery time, 50 μs, to suppress acoustic ringing. Pulse delays of 60 s were employed. Samples were prepared by loading a spinner with a Teflon spacer followed by ca. 65 mg of sample and 15 mg of tetrakis-(trimethylsilyl)silane (TTMS), followed by an additional 65 mg of sample, and a sample end spacer. Chemical shifts were referenced to internal TTMS.

(b) BET. The N_2 adsorption/desorption isotherms were obtained from a Quantachrome BET instrument (Autosorb-6). The Brunauer−Emmett−Teller (BET) surface area of the pure silica was found to be 886−928 m^2/g (depending on batch), and the BET surface of the functionalized silica is approximately half this value, depending upon the degree of coverage. The pore size is estimated from the desorption branch, using a standard Barrett−Joyner−Halenda (BJH) method.

(c) ICP-MS. For non-radioactive samples, solution metal concentrations were determined using ICP-MS, on a Hewlett-Packard HP4500. Solutions were acidified using either HCl or HNO_3.

Batch Contacts with Actinide Solutions. Solutions of 1 M $NaNO_3$ were prepared from reagent-grade chemicals. Concentrated HNO_3 was added on a volume basis to make 1 M $NaNO_3$−0.1 M HNO_3 solution. Additionally concentrated HNO_3 was titrated into aliquots of 1 M $NaNO_3$ to pH end points 4, 2, and 1 as indicated potentiometrically. Aliquots of these solutions were spiked with ^{230}Th, ^{237}Np, ^{241}Am(III), ^{239}Pu(IV), or ^{233}U(VI) resulting in nominal 2000 dpm/mL concentrations. The radiotracers ^{233}U (0.15 M HNO_3), ^{239}Pu (7 M HNO_3), and ^{241}Am (0.01 M HNO_3) were obtained from in-house stocks. Interference test solutions were prepared by adding aliquots of 10 mg/mL standard solutions to aliquots of 1 M $NaNO_3$−0.1 M HNO_3. The solution/solid ratio was varied from 50 to 5000 to explore the effect on binding efficiency. No significant variation was observed over this range, so a solution-to-solids ratio of 100 was adopted as standard. Samples were shaken in an orbital shaker for 1−4 h (control experiments revealed that equilibrium was reached in less than 30 min, so these results represent true equilibrium conditions). After the mixtures were shaken for the specified time, they were filtered through a 0.2 μm syringe filter. Test solution aliquots were suspended in Ultima Gold (Packard Instrument, Meriden, CT) scintillation cocktail, and α activities were measured using a 2550 TR/AB liquid scintillation counter (Packard Instruments). In the cases where ^{241}Am-(III) and ^{239}Pu(IV) were tested in the same contact solution, the isotope-specific activity was determined using α energy analysis on a precipitation-plated mount. Experiments were also performed in which competing ions and complexants were included in the mélange.

Kinetics. The kinetics experiments were performed similarly to the batch contacts. The test solution was 1 M $NaNO_3$−0.1 M HNO_3. Sample aliquots were removed at the specific time intervals ranging from 1 min to 6 h. At specific time intervals, aliquots (1 vol %) were removed, filtered through 0.2 μm filters, and counted using liquid scintillation.

Results and Discussion

Synthesis. We employed three related synthetic pathways to prepare our functionalized SAMMS materials, exemplifying the versatility of our convergent SAMMS synthesis. Glycinyl-urea SAMMS were prepared by treating an isocyanate

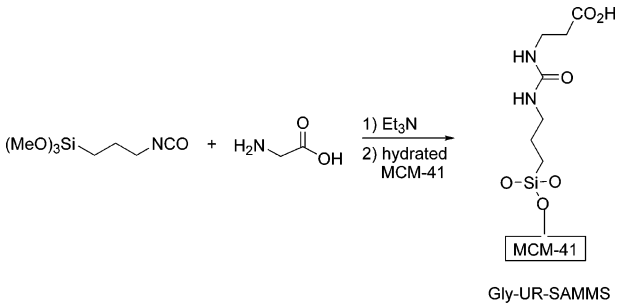

FIGURE 2. Preparation of glycinyl-urea (Gly-UR) SAMMS.

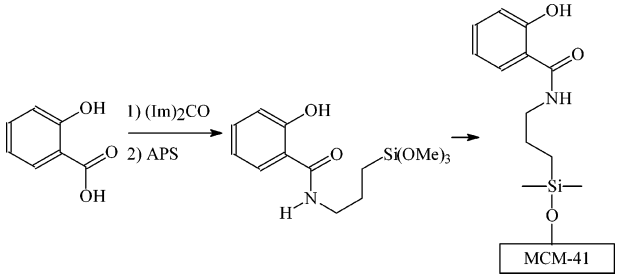

FIGURE 3. Preparation of the salicylamide ligand.

terminated silane with a triethylamine-buffered solution of glycine. This approach tethers the acid to the silane via a urea linkage (see Figure 2). In this fashion, we obtained a glycine terminated SAMMS material with a surface coverage of approximately 4.0 silanes/nm^2 (as determined by solid-state ^{29}Si NMR).

The second of our strategies is exemplified by the incorporation of the salicylate ligand via an amide linkage to commercially available aminopropylsiloxane (APS), accomplished by activating the carboxylate with carbonyl diimidazole (see Figure 3). All attempts to effect this amidation via the corresponding methyl and ethyl esters failed. The CDI amidation reaction was followed immediately by deposition in freshly hydrated MCM-41. This protocol resulted in the deposition of 1.1 silanes/nm^2, which is the expected level of coverage for an aromatic terminated silane of this bulk. This strategy was also used to make the *p*-NO_2 analogue and other related aromatic interfaces, resulting in similar coverage densities.

The third synthetic route was used to prepare the phosphonate SAMMS and involved displacement of trifluoroethanol from the corresponding ester, as shown in Figure 4 (*45*). This silane achieved a surface coverage of 2.0−2.2 silanes/nm^2.

Distribution Coefficient Measurements. The actinide target species commonly form insoluble hydroxides or polymeric oxides under alkaline conditions, so our binding studies were performed over a pH range of 1.0−6.5. Cation binding is an equilibrium process and can be influenced by the stoichiometric ratio of binding sites to solution cation content. The solution/solids ratio employed in these experiments was typically 200 but was also studied in a range from 50 to 1000. To ensure that all distribution coefficients reflected genuine equilibrium conditions, contact times were several hours (typically 1−4; as will be shown later, equilibrium under these conditions is reached within only a few minutes):

$$K_d = \frac{(C_o - C_f)}{C_f} \times \frac{V}{M}$$

The distribution coefficients (K_d) are simply a mass-weighted partition coefficient between the aqueous supernatant phase and SAMMS solid phase. The higher the K_d value, the more effective the sorbent material is at sequestering the target species. For an arbitrarily chosen solution-to-solids ratio of 100 (i.e., 1% sorbent loading), a K_d of 1000 indicates that 10 times as much of the target analyte is in the sorbent phase as is left in the supernatant solution (in other words, 90% sequestration). K_d values above 500 are considered acceptable, those above 5000 are considered very good, and K_d values in excess of 50 000 are considered outstanding. The units of K_d in this case are mL/g. The uncertainty of the K_d values obtained in these studies is estimated to be ±5%.

Binding Studies. Much has been learned in terms of metal−ligand interactions from actinide solvent extraction studies, as well as those studies aimed at designing ligands to remove actinides from biological systems. The key lessons arising from these studies are that the actinide cations are hard Lewis acids that are considerably larger than the typical transition metal cation and that ligand synergy is an important attribute to design into a ligand field. Noteworthy examples of how these concepts have been joined into powerful rare earth ligand systems include the hydroxyp-

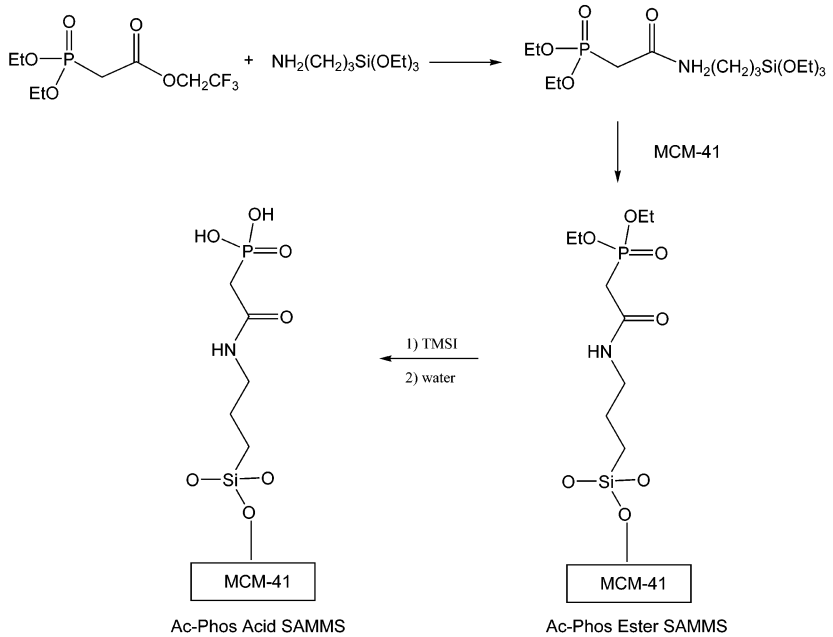

FIGURE 4. Preparation of acetamide-phosphonate ("Ac-Phos") acid SAMMS.

ridinone (HOPO) and desferrioxamine (DFO) chelators (*46*−*48*) and the carbamoylphosphine oxide (CMPO) extractants (*49*, *50*). Our previous lanthanide model studies suggested that SAMMS are a viable method for sequestering actinides and that the synergistic ligand field concept outlined above is indeed valid at the monolayer interface inside a mesoporous matrix.

Salicylamide. One of the simplest and most direct entries into a synergistic ligand field is provided by the salicylamide ligand due to the combination of the resonance stabilized phenolic OH group and the adjacent amide carbonyl group. Salicylamide-based ligands have been used to chelate a wide variety of metal cations (*51*−*53*), and recently salicylamide-based ligand systems have been very elegantly employed to create elaborate supermolecular complexes (*54*). The pH limitation found with this ligand was initially thought to arise from the modest acidity of the phenolic hydroxyl group. As a means of testing this hypothesis, we also prepared and studied the 5-nitro analogue as well as phthalamide SAMMS (the corresponding ortho carboxylic acid). Neither one of these more acidic ligands demonstrated any notable improvement over the original Sal-SAMMS.

Eu(III) was chosen as a model system to mimic the Am(III). Detailed EXAFS analysis of the Eu(III) adduct of Sal-SAMMS revealed an average Eu−O coordination number of 8 ± 1.2, a Eu−O radial distance of 2.40 ± 0.015 Å, and an XAFS Debye−Waller term of 0.0145 ± 0.0025 $Å^{-2}$. These results are consistent with the Eu(III) cation being 8-coordinate (not unusual for the lanthanides), in either a cubic or distorted square antiprism geometry. Taking into account the geometric considerations of the monolayer interface, a distorted square antiprism is the most likely bonding geometry for this complex. These EXAFS results clearly support the conclusion that the close proximity of the ligands in the monolayer interface allows for multiple ligands to interact with a single metal cation. In this case we observe a 4:1 ligand:metal interaction, which clearly contributes to enhancing the binding affinity between a given ligand and metal cation.

Glycinyl-Urea. The rigid nature of the benzene ring precludes coplanar chelation of the metal cation if the ionic radius of the cation is large (as with the early lanthanides and low oxidation state actinides). Thus, we chose to explore the conformationally more flexible sp^3 hybridized ligand systems, in conjunction with seven-membered chelates.

While the actinide binding affinity of the salicylamide SAMMS was found to be modest at best, the glycinyl-urea SAMMS were found to be far more effective. However, the binding is heavily dependent on pH, with the better binding efficiencies occurring at higher pH values, with binding affinity for the actinides dropping off below a pH of 2. This is not unexpected because of the basicity of the carboxylate ligand. However, as a result of the ubiquitous nature and low cost associated with carboxylate ligands (e.g., glycine derivatives) and the fact that they function well in the pH range of 2−4, these ligands may offer a cost-effective compromise for sequestering actinides from complex mixtures. In summary, Gly-UR SAMMS were found to bind all of the actinides studied, except for Np(V), which is difficult to sequester (see Table 1) and Gly-UR SAMMS were found to have a broader pH window, effectively binding the target actinides to below a pH of 4. The conformationally flexible Gly-UR SAMMS were also found to bind both large and small cations with relative ease.

The ability to regenerate any sorbent material is a key factor in determining life cycle costs and field application strategy. The fact that these carboxylate SAMMS show lesser K_d values at lower pH values suggests that it might be possible to strip the target species from the SAMMS phase with an acid wash. To test this, we studied regeneration using Eu(III) as a model system. This was done by stripping the sorbed europium with an acid wash (0.5 M HCl) and re-exposing the SAMMS to fresh europium solution, and then we re-measured the sorption affinity. Repeating this cycle 10 times revealed no loss in binding affinity (see Table 2). Clearly, regeneration of Gly-UR SAMMS is both easy and effective, making recycling of these nanostructured sorbent materials a viable option in their deployment.

TABLE 1. Actinide Distribution Coefficient Values for the Carboxylic Acid SAMMS[a]

actinide	pH	K_d (mL/g) Phthal-SAMMS	K_d (mL/g) Gly-UR SAMMS
Am(III)	0.78	0	0
	1.9	0	1
	4.26	51	92 000
	5.24	1 400	240 000
Pu(IV)	0.66	0	160
	1.05	46	5 100
	2.08	9 000	45 000
Np(V)	0.72	0	0
	1.55	0	0
	3.68	0	86
	4.73	0	200
U(VI)	0.7	57	160
	2.36	130	12 000
	4.55	2 800	160 000
Th(IV)	0.76	34	900
	2.43	2 000	91 000

[a] [Ac] = 2000 dpm/mL. 0.1 M $NaNO_3$. 0.10 g SAMMS in 10 mL.

TABLE 2. Acid Regeneration of Glycinyl-Urea SAMMS and Eu(III) Binding Affinity[a]

cycle	C_{ini} (ppb)	C_{fin} (ppb)	K_d (mL/g)
1	1708	76	4300
2	1800	73	4700
3	1922	88	4200
4	1826	74	4700
5	1730	57	5900
6	1892	50	7400
7	1870	50	7300
8	1742	49	6900
9	1814	67	5200
10	1438	43	6500

[a] At pH 4.

Phosphonate Ligands. Ac-Phos and Prop-Phos ester SAMMS have both the carbonyl amide and the P═O ester ligands incorporated as a part of the monolayer interface. Both of these groups activate the central enolizable methylene, creating the protic portion of the ligand (similar to the classic acetonylacetonate, or acac, ligand). The ambiphilic wettability of the phosphonate ester interface makes these SAMMS materials particularly well-suited for sequestering species from nonaqueous waste streams (e.g., oils, cutting fluids, solvents, etc.).

The homologation of Ac-Phos ester SAMMS to form Prop-Phos ester SAMMS does two things. First, it significantly attenuates the acidity of the enolizable methylene, and second it increases the chelate ring size to 7. In a series of neutral diamide ligands designed as solution extractants, seven-membered chelates are known to effectively ligate the lanthanide cations (*55*).

The Ac-Phos ester was found to be effective for all of the actinides studied, except for the difficulty to bind Np(V) (see Table 3). Distribution coefficients were commonly found to be in excess of 20 000 and in some cases over 200 000. In contrast, the Prop-Phos ester was found to be selective for Pu(IV), and especially so at low pH values. In fact, it is possible

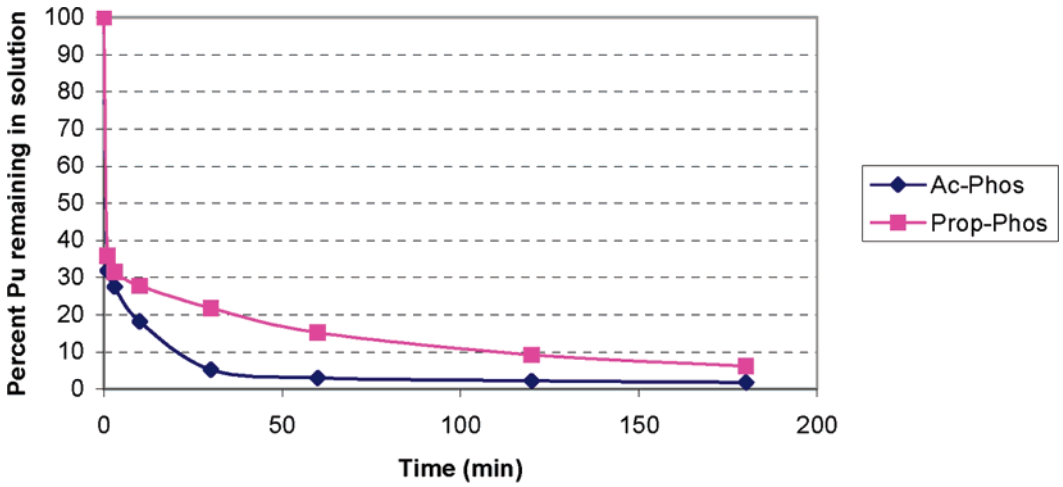

FIGURE 5. Kinetics of Pu(IV) sorption using the phosphonate ester SAMMS.

TABLE 3. Actinide Distribution Coefficients for the Phosphonate Ester SAMMS[a]

actinide	pH	K_d (mL/g) Ac-Phos SAMMS diethyl ester	K_d (mL/g) Prop-Phos SAMMS diethyl ester
Am(III)	0.78	600	0
	1.9	3 900	0
	4.26	210 000	33
	5.24	460 000	48
Pu(IV)	0.66	94 000	61 000
	1.05	72 000	66 000
	2.08	52 000	36 000
Np(V)	0.72	60	0
	1.55	55	0
	3.68	43	0
	4.73	150	0
U(VI)	0.7	26 000	170
	2.36	31 000	1 400
	4.55	24 000	12 000
Th(IV)	0.76	23 000	21 000
	2.43	13 000	31 000

[a] [Ac] = 2000 dpm/mL. 0.1 M $NaNO_3$. 0.20 g SAMMS in 10 mL.

to easily and almost quantitatively separate Pu(IV) and Am(III) at low concentrations with a single simple treatment with Prop-Phos ester SAMMS.

The phosphonate esters were cleaved using trimethylsilyl iodide (TMSI) in anhydrous acetonitrile (or pure, in the vapor phase), followed by hydrolysis to afford the corresponding phosphonic acids. Both of these new phosphonic acid SAMMS were found to be exceptionally good actinide scavengers with distribution coefficients of 15 000−20 000 commonly being observed (see Table 6). For a solution-to-solids ratio of 100 (i.e., a 1% solids loading), this indicates that more than 99% of the target actinide is captured in the SAMMS phase.

Kinetics Studies. The K_d values are a measure of the thermodynamic equilibrium of actinide binding affinity. However, even the highest actinide binding affinity is useless in the real world if it takes a long time to reach equilibrium. Therefore, the sorption kinetics for Pu(IV) binding were systematically studied for the Ac-Phos and Prop-Phos SAMMS, in both their ester and acid forms. The data shown below for the phosphonate ester SAMMS binding of Pu(IV) indicate that equilibrium is reached in 1−2 h (see Figure 5). This is notably slower than for other binding studies using SAMMS terminated with protic and/or ionic ligand fields (*32*−*37*, *43*). We believe that this is due to the fact that Pu(IV) is known to form strong complexes with nitrate anion, and

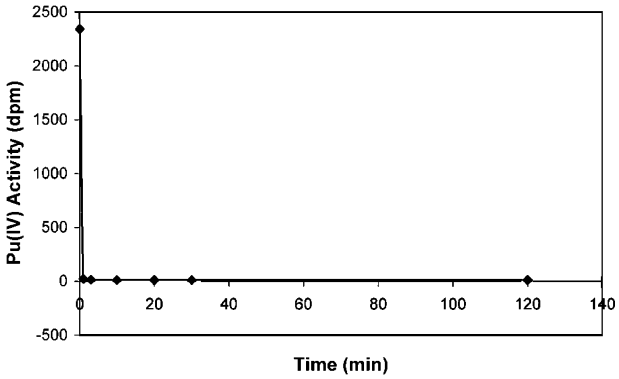

FIGURE 6. Sorption kinetics of Pu(VI) using Prop-Phos acid SAMMS.

the neutral Ac-Phos ligand has trouble competing with nitrate anion for the Pu(IV) cation, making the initial binding interaction slow. However, once bound by the first Ac-Phos ligand, the high local concentration and close proximity of the ligands allows for multiligand chelation of the Pu(IV) cation and hence a strong binding affinity overall.

In contrast, the binding kinetics of the phosphonic acid SAMMS was found to be exceptionally rapid (see Figure 6). The protic/ionic nature of the interfacial ligand field allows it to compete very effectively with nitrate anion for the Pu(IV) cation. It is apparent from these data that diffusion into the mesoporous matrix is not a significant kinetic limitation. Note that no Pu leaching is observed upon prolonged reaction times.

Nitrate Dependence. It became apparent during the course of these studies that the K_d values for Pu with various SAMMS tended to vary somewhat depending on the nitrate concentration of the solution matrix. Thus, we explored this effect in detail. The data are summarized in Figure 7. As can be seen, the K_d values tend to be quite high at low nitrate concentrations (commonly 50 000−200 000) and decrease with increasing nitrate concentration up to approximately 1 M nitrate, beyond which the K_d values level off with no further attenuation. It has been known for some time that Pu forms strong complexes with nitrate anion (*56*) and that competition is thought to be the source of this K_d attentuation. While this is indeed a concern in terms of the ultimate implementation of SAMMS for Pu separations, it must be noted that the effect does level off above 1 M nitrate and that the K_d values are still on the order of 10 000−20 000, making this a strong separations method despite this effect.

Competition Studies. Competition studies carried out with the phosphonate ester SAMMS reveal modest competi-

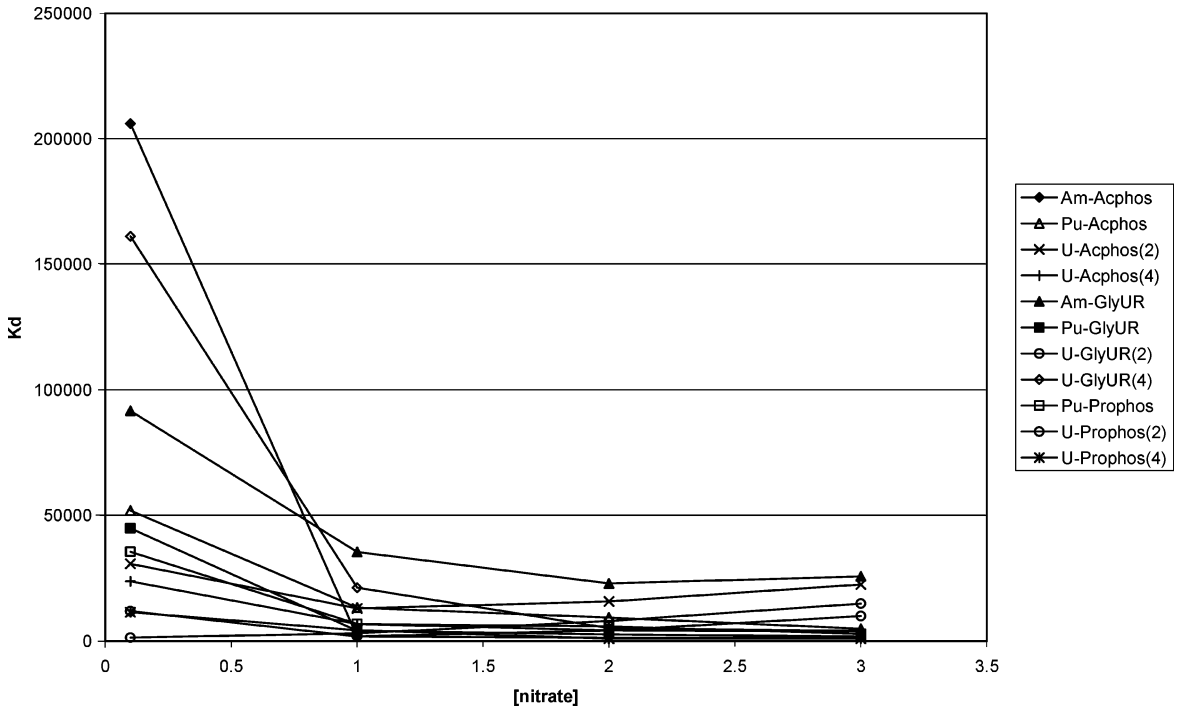

FIGURE 7. Actinide SAMMS distribution coefficient dependence on nitrate concentration.

TABLE 4. %Pu (IV) Competition Studies with Phosphonate Ester SAMMS[a]

competitor	concentration	K_d (Pu) Ac-Phos diethyl ester (mL/g)	K_d (Pu) Prop-Phos diethyl ester (mL/g)
none		11 000	4 200
Fe(III)	100 ppm	6 000	2 900
Al(III)	100 ppm	9 900	4 000
Zr(IV)	100 ppm	9 700	560
Ni(II)	100 ppm	11 000	4 600
Ca(II)	100 ppm	10 000	4 100
Mn(II)	100 ppm	8 400	2 200
Mo(VI)	100 ppm	8 600	4 800
Cu(II)	100 ppm	9 300	4 100
Pb(II)	100 ppm	12 000	4 200
Cr(III)	100 ppm	11 000	4 000
Hg(II)	100 ppm	10 000	4 200
phosphate	0.01 M	10 000	3 700
sulfate	0.01 M	11 000	3 400
EDTA	0.01 M	59	4
citrate	0.01 M	12 000	2 200

[a] [Pu] = 2000 dpm/mL. 1 M $NaNO_3$. 0.1 M HNO_3.

TABLE 5. Uranium Competition Studies with Phosphonate Ester SAMMS[a]

competitor	concentration	K_d (U) Ac-Phos diethyl ester (mL/g)	K_d (U) Prop-Phos diethyl ester (mL/g)
none		12 000	210
Fe(III)	100 ppm	1 600	64
Al(III)	100 ppm	11 000	210
Zr(IV)	100 ppm	13 000	120
Ni(II)	100 ppm	11 000	570
Ca(II)	100 ppm	15 000	450
Mn(II)	100 ppm	13 000	250
Mo(VI)	100 ppm	10 000	80
Cu(II)	100 ppm	12 000	410
Pb(II)	100 ppm	16 000	200
Cr(III)	100 ppm	12 000	210
Hg(II)	100 ppm	16 000	150
phosphate	0.01 M	12 000	250
sulfate	0.01 M	12 000	320
EDTA	0.01 M	14 000	350
citrate	0.01 M	13 000	310

[a] [U] = 2000 dpm/mL. 1 M $NaNO_3$. 0.1 M HNO_3. 0.10 g SAMMS in 10 mL.

tion from ferric ion (see Table 4). In addition, there is an interesting anionic competition noted for both Pu (with zirconate). It is worth noting that our previous lanthanide scoping studies suggested that Prop-Phos ester SAMMS would be a poor actinide scavenger, and that is indeed the case for U(VI); however, the Pu(IV) affinity is still moderately high, revealing some the limitations of using lanthanides to model actinide binding.

In the Pu (IV) competition studies, a severe competitive interaction observed was with EDTA, which seriously attenuated the binding affinity of both the Ac-Phos and Prop-Phos ester SAMMS. A similar series of experiments was carried out for U(VI), and once again it was found that Fe(III) offered some significant competition (see Table 5). In addition, modest competition was found with molybdate anion.

In contrast to the esters, the phosphonic acid SAMMS show no interference whatsoever from either competing transition metal cations or complexants (see Table 6). The Pu(IV) binding affinity remains high in the presence of a wide variety of competitors. It should be noted that these kinetics were carried out with high nitrate concentrations, revealing that the phosphonic acid SAMMS can compete with nitrate, as well as EDTA, very effectively.

Recently the U.S. DOE has placed emphasis on the need to significantly reduce the volume of material put through the waste vitrification process. SAMMS has demonstrated the ability to selectively sequester actinides from complex mixtures, offering one potential method for significantly reducing the volume of waste for vitrification. The rigid open pore structure allows for facile diffusion into the mesoporous matrix, providing for fast sequestration kinetics. SAMMS, being a silica-based chemical separation method, is completely amenable to vitrification and could be used to significantly reduce the volume of waste to be vitrified since only the volume of the radionuclide-laden SAMMS would

TABLE 6. Pu(IV) Competition Studies Using Phosphonic Acid SAMMS[a]

competitor	concentration	K_d (Pu) Ac-Phos acid form (mL/g)	K_d (Pu) Prop-Phos acid form (mL/g)
none		21 000	16 000
Fe(III)	100 ppm	21 000	14 000
Al(III)	100 ppm	29 000	11 000
Zr(IV)	100 ppm	20 000	16 000
Ni(II)	100 ppm	20 000	16 000
Ca(II)	100 ppm	20 000	16 000
Mn(II)	100 ppm	18 000	16 000
Mo(VI)	100 ppm	19 000	13 000
Cu(II)	100 ppm	19 000	16 000
Pb(II)	100 ppm	20 000	18 000
Cr(III)	100 ppm	18 000	15 000
Hg(II)	100 ppm	16 000	16 000
phosphate	0.01 M	20 000	18 000
sulfate	0.01 M	20 000	18 000
EDTA	0.01 M	20 000	16 000
citrate	0.01 M	23 000	19 000

[a] [Pu] = 2000 dpm/mL. 1 M $NaNO_3$. 0.1 M HNO_3. 0.10 g SAMMS in 10 mL.

have to be vitrified and not the vast bulk of the waste. As a result of this substantial HLW volume reduction, the potential cost savings offered by SAMMS to the the U.S. DOE cleanup effort is considerable.

Acknowledgments

This research was supported by the U. S. Department of Energy (DOE), Environmental Management Science Program. Portions of this work were performed at Pacific Northwest National Laboratories, which is operated for the DOE by Battelle Memorial Institute under Contract DE AC06-76RLO 1830. Portions of this work were performed at the Materials Research Collaborative Access Team (MRCAT) at the Advanced Photon Source. MRCAT is supported by the Department of Energy under Contract DE-FG02-94-ER45525 and the member institutions. Use of the Advanced Photon Source was supported by the U.S. Department of Energy, Basic Energy Sciences, Office of Energy Research under Contract W-31-102-Eng-38.

Literature Cited

(1) Antochshuk, V.; Olkhovyk, O.; Jaroniec, M.; Park, I.-S.; Ryoo, R. Benzoylthiourea-modified mesoporous silica for mercury(II) removal. *Langmuir* **2003**, *19*, 3031−3034.

(2) Antochshuk, V.; Jaroniec, M. Functionalized Mesoporous Materials obtained via interfacial reactions in self-assembled silica-surfactant systems. *Chem. Mater.* **2000**, *12*, 2496−2501.

(3) Antochshuk, V.; Araujo, A. S.; Jaroniec, M. Functionalized MCM-41 and CeMCM-41 materials synthesized via interfacial reactions. *J. Phys. Chem. B* **2000**, *104*, 9713−9719.

(4) Antochshuk, V.; Kruk, M.; Jaroniec, M. Surface modifications of cage-like and channel-like mesopores and their implications for evaluation of sizes of entrances to cage-like mesopores. *J. Phys. Chem. B* **2003**, *107*, 11900−11906.

(5) Zhang, Z.; Dai, S.; Fan, X.; Blom, D. A.; Pennycook, S. J.; Wei, Y. Controlled synthesis of CdS nanoparticles inside ordered mesoporous silica using ion-exchange reaction. *J. Phys. Chem. B* **2001**, *105*, 6755−6758.

(6) Ju, Y. H.; Webb, O. F.; Dai, S.; Lin, J. S.; Barnes, C. E. Synthesis and characterization of ordered mesoporous anion-exchange inorganic/organic hybrid resins for radionuclide separation. *Ind. Eng. Chem. Res.* **2000**, *39*, 550−553.

(7) Zhang, Z.; Dai, S. Preparation and characterization of novel inorganic−organic mesoscopic ordered composites with bridges formed by coordination compounds. *J. Am. Chem. Soc.* **2001**, *123*, 9204−9205.

(8) Dai, S.; Burleigh, M. C.; Ju, Y. H.; Gao, H. J.; Lin, J. S.; Pennycook, S. J.; Barnes, C. E.; Xue, Z. L. Hierarchically imprinted sorbents for the separation of metal ions. *J. Am. Chem. Soc.* **2000**, *122*, 992−993.

(9) Im, H.-J.; Yang, Y.; Allain, L. R.; Barnes, C. E.; Dai, S.; Xue, Z. Functionalized sol−gels for selective copper(II) separation. *Environ. Sci. Technol.* **2000**, *34*, 2209−2214.

(10) Mori, Y.; Pinnavaia, T. J. Optimizing organic functionality in mesostructured silica: direct assembly of mercaptopropyl groups in wormhole framework structures. *Chem. Mater.* **2001**, *13*, 2173−2178.

(11) Mercier, L.; Pinnavaia, T. J. Direct synthesis of hybrid organic−inorganic nanoporous silica by a neutral amine assembly route: structure−function control by stoichiometric incorporation of organosiloxane molecules. *Chem. Mater.* **2000**, *12*, 188−196.

(12) Mercier, L.; Pinnavaia, T. J. Heavy metal ion adsorbents formed by the grafting of a thiol functionality to mesoporous silica molecular sieves: factors affecting Hg(II) uptake. *Environ. Sci. Technol.* **1998**, *32*, 2749−2754.

(13) Burleigh, M. C.; Markowitz, M. A.; Spector, M. S.; Gaber, B. P. Direct synthesis of periodic mesoporous organosilicas: functional incorporation by co-condensation with organosilanes. *J. Phys. Chem. B* **2001**, *105*, 9935−9942.

(14) Asefa, T.; Kruk, M.; MacLachlan, M. J.; Coombs, N.; Grondey, H.; Jaroniec, M.; Ozin, G. A. Novel bifunctional periodic mesoporous organosilicas, BPMOs: synthesis, characterization, properties and in-situ selective hydroboration-alcoholysis reactions of functional groups. *J. Am. Chem. Soc.* **2001**, *123*, 8520−8530.

(15) Richer, R.; Mercier, L. Direct synthesis of functional mesoporous silica by neutral pH nonionic surfactant assembly: factors affecting framework structure and composition. *Chem. Mater.* **2001**, *13*, 2999−3008.

(16) Walcarius, A.; Delacote, C. Rate of access to the binding sites in organically modified silicates. 3. Effect of structure and density of functional groups in mesoporous solids obtained by the co-condensation route. *Chem. Mater.* **2003**, *15*, 4181−4192.

(17) Kruk, M.; Asefa, T.; Jaroniec, M.; Ozin, G. A. Metamorphosis of ordered mesopores to micropores: periodic silica with unprecedented loading of pendant reactive organic groups transforms to periodic microporous silica with tailorable pore size. *J. Am. Chem. Soc.* **2002**, *124*, 6383−6392.

(18) Sinlapadech, S.; Krishna, R. M.; Luan, Z.; Kevan, L. Photoionization of *N*-alkylphenothiazines in mesoporous Me-AlMCM-41 containing transition metal ions Me = Ni(II), Fe(III), and Cu(II). *J. Phys. Chem. B* **2001**, *105*, 4350−4355.

(19) Luan, Z.; Bae, J. Y.; Kevan, L. Vanadosilicate mesoporous SBA-15 molecular sieves incorporated with *N*-alkylphenothiazines. *Chem. Mater.* **2000**, *12*, 3202−3207.

(20) Ranjit, K. T.; Bae, J. Y.; Chang, Z.; Kevan, L. Photoionization of methylphenothiazine in palladium ion-exchanged SAPO-5 and SAPO-11 silicoaluminophosphate microporous materials at room temperature. *J. Phys. Chem. B* **2002**, *106*, 583−588.

(21) Krishna, R. M.; Prakash, A. M.; Kevan, L. Photoionization of *N*-alkylphenothiazines in mesoporous SiMCM-41, AlMCM-41, and TiMCM-41 molecular sieves. *J. Phys. Chem. B* **2000**, *104*, 1796−1801.

(22) Chang, Z.; Kevan, L. Photoionization of tetraphenylporphyrin in mesoporous SiMCM-48, AlMCM-48, and TiMCM-48 molecular sieves. *Langmuir* **2002**, *18*, 911−916.

(23) Ranjit, K. T.; Kevan, L. Photoinduced charge separation of pyrene in chromium containing silicoaluminophosphate (SAPO-5) microporous materials at room temperature. *J. Phys. Chem. B* **2003**, *107*, 2610−2617.

(24) Murali, A.; Chang, Z.; Ranjit, K. T.; Krishna, R. M.; Kurshev, V.; Kevan, L. Structural characterization and study of adsorbate interactions with Cu(II) ions in SBA-15 materials by electron spin resonance and electron spin−echo modulation spectroscopies. *J. Phys. Chem. B* **2002**, *106*, 6913−6920.

(25) Zhu, Z.; Hartmann, M.; Maes, E. M.; Czernuszewicz, R. S.; Kevan, L. Physicochemical characterization of chromium oxides immobilized in mesoporous MeMCM-41 (Me = Al, Ti, and Zr) molecular sieves. *J. Phys. Chem. B* **2000**, *104*, 4690−4698.

(26) Schroden, R. C.; Blanford, C. F.; Melde, B. J.; Johnson, B. J. S.; Stein, A. Direct synthesis of ordered macroporous silica materials functionalized with polyoxometalate clusters. *Chem. Mater.* **2001**, *13*, 1074−1081.

(27) Aronson, B. J.; Blanford, C. F.; Stein, A. Synthesis, characterization, and ion-exchange properties of zinc and magnesium manganese oxides confined within MCM-41 channels. *J. Phys. Chem. B* **2000**, *104*, 449−459.

(28) Johnson, B. J. S.; Stein, A. Surface modification of mesoporous, macroporous, and amorphous silica with catalytically active polyoxometalate clusters. *Inorg. Chem.* **2001**, *40*, 801−808.
(29) Liu, J.; Shin, Y.; Nie, Z.; Chang, J. H.; Wang, L.-Q.; Fryxell, G. E.; Samuels, W. D.; Exarhos, G. J. Molecular assembly in ordered mesoporosity: a new class of highly functional nanoscale materials. *J. Phys. Chem. A* **2000**, *104*, 8328−8339.
(30) Fryxell, G. E.; Liu, J. Designing surface chemistry in mesoporous silica. In *Adsorption at Silica Surfaces*; Papirer, E., Ed.; Marcel Dekker: New York, 2000.
(31) Moller, K.; Bein, T. Inclusion chemistry in periodic mesoporous hosts. *Chem. Mater.* **1998**, *10*, 2950−2963.
(32) Feng, X.; Fryxell, G. E.; Wang, L. Q.; Kim, A. Y.; Liu, J. Organic monolayers on ordered mesoporous supports. *Science* **1997**, *276*, 923−926.
(33) Chen, X.; Feng, X.; Liu, J.; Fryxell, G. E.; Gong, M. Mercury separation and immobilization using self-assembled monolayers on mesoporous supports (SAMMS). Proceedings of the 10th Symposium on Separation Science and Technology for Energy Applications, October 20−24, 1997, Gatlinburg, TN.
(34) Liu, J.; Feng, X.; Fryxell, G. E.; Wang, L. Q.; Kim, A. Y.; Gong, M. Hybrid mesoporous materials with functionalized monolayers. *Adv. Mater.* **1998**, *10*, 161−165.
(35) Yantasee, W.; Lin, Y.; Zemanian, T. S.; Fryxell, G. E. Voltametric detection of lead(II) and mercury(II) using a carbon paste electrode modified with thiol self-assembled monolayer on mesoporous silica (SAMMS). *Analyst* **2003**, *128*, 467−472.
(36) Kemner, K.; Feng, X.; Liu, J.; Fryxell, G. E.; Wang, L.-Q.; Kim, A. Y.; Gong, M.; Mattigod, S. Investigation of the local chemical interactions between Hg and self-assembled monolayers on mesoporous supports. *J. Synchrotron Radiat.* **1999**, *6*, 633−635.
(37) Mattigod, S. V.; Feng, X.; Fryxell, G. E.; Liu, J.; Gong, M. Separation of complexed mercury from aqueous wastes using self-assembled mercaptan on mesoporous silica. *Sep. Sci. Technol.* **1999**, *34*, 2329−2345.
(38) Fryxell, G. E.; Liu, J.; Mattigod, S. Environmental applications of self-assembled monolayers on mesoporous supports (SAMMS). *Mater. Technol.* **1999**, *14*, 188−191.
(39) Fryxell, G. E.; Liu, J.; Gong, M.; Hauser, T. A.; Nie, Z.; Hallen, R. T.; Qian, M.; Ferris, K. F. Design and synthesis of selective mesoporous anion traps. *Chem. Mater.* **1999**, *11*, 2148−2154.
(40) Kelly, S.; Kemner, K.; Fryxell, G. E.; Liu, J.; Mattigod, S. V.; Ferris, K. F. An X-ray absorption fine structure spectroscopy study of the interactions between contaminant tetrahedral anions to self-assembled monolayers on mesoporous supports. *J. Phys. Chem.* **2001**, *105*, 6337−6346.
(41) Yoshitake, H.; Yokoi, T.; Tatsumi, T. Adsorption of chromate and arsenate by amino-functionalized MCM-41 and SBA-1. *Chem. Mater.* **2002**, *14*, 4603−4610.
(42) Yoshitake, H.; Yokoi, T.; Tatsumi, T. Adsorption behavior of arsenate at transition metal cations captured by amino-functionalized mesoporous silicas. *Chem. Mater.* **2003**, *15*, 1713−1721.
(43) Lin, Y.; Fryxell, G. E.; Wu, H.; Englehard, M. Selective sorption of cesium using self-assembled monolayers on mesoporous supports (SAMMS). *Environ. Sci. Technol.* **2001**, *35*, 3962−3966.
(44) Mattigod, S. V.; Fryxell, G. E.; Serne, R. J.; Parker, K. E.; Mann, F. M. Evaluation of novel getters for adsorption of radioiodine from groundwater and waste glass leachates. *Radiochim. Acta* **2003**, *91*, 539−545.
(45) Birnbaum, J. C.; Busche, B.; Shaw, W. J.; Fryxell, G. E. Synthesis of carbamoylphosphonate silanes for the selective sequestration of actinides *Chem. Commun.* **2002**, 1374−1375.
(46) Xu, J.; Raymond, K. N. Uranyl sequestering agents: correlation of properties and efficacy with structure for UO_2^{2+} complexes of linear tetradentate 1-methyl-3-hydroxy-2(1*H*)-pyridinone ligands. *Inorg. Chem.* **1999**, *38*, 308−315.
(47) Lambert, T. N.; Dasaradhi, L.; Huber, V. J.; Gopalan, A. S. Synthesis of 3-hydroxy-2-pyridinone derivatives of 4-*tert*-butylcalix[4]arenes: a new class of selective extractants of actinide(IV) ions. *J. Org. Chem.* **1999**, *64*, 6097−6101.
(48) Whisenhunt, D. W.; Neu, M. P.; Hou, Z.; Xu, J.; Hoffman, D. C. Raymond, K. N. Specific sequestering agents for the actinides. 29. Stability of the thorium(IV) complexes of desferrioxamine B (DFO) and three octadentate catecholate or hydroxypyridinonate DFO derivatives: DFOMTA, DFOCAMC, and DFO-1,2-HOPO. Comparative stability of the plutonium(IV) DFOMTA complex. *Inorg. Chem.* **1996**, *35*, 4128−4136.
(49) Lambert, T. N.; Jarvinen, G. D.; Gopalan, A. S. Syntheses of some new polyaminocarboxylate and CMPO calix[4]arene chelators for the selective extraction of actinide ions. *Tetrahedron Lett.* **1999**, *40*, 1613−1616.
(50) Michael, K. M.; Rizvi, G. H.; Mathur, J. N.; Kapoor, S. C.; Ramanujam, A.; Iyer, R. H. Recovery of plutonium and americium from laboratory acidic waste solutions using tri-*n*-octylamine and octylphenyl-*N*,*N*-diisobutylcarbamoylmethylphosphine oxide. *Talanta* **1997**, *44*, 2095−2102.
(51) Cohen, S. M.; Raymond, K. N. Catecholate/salicylate heteropodands: demonstration of a catecholate to salicylate coordination change. *Inorg. Chem.* **2000**, *39*, 3624−3631.
(52) Cohen, S. M.; Petoud, S.; Raymond, K. N. A novel salicylate-based macrobicycle with a "split personality". *Inorg. Chem.* **1999**, *38*, 4522−4529.
(53) Cohen, S. M.; Meyer, M.; Raymond, K. N. Enterobactin protonation and iron release: hexadentate tris-salicylate ligands as models for triprotonated ferric enterobactin. *J. Am. Chem. Soc.* **1998**, *120*, 6277−6286.
(54) Caulder, D. L.; Raymond, K. N. Supermolecules by design. *Acc. Chem. Res.* **1999**, *32*, 975−982.
(55) Rapko, B. M.; McNamara, B. K.; Rogers, R. D.; Lumetta, G. J.; Hay, B. P. Coordination of lanthanide nitrates with *N*,*N*,*N*′,*N*′-tetramethylsuccinamide. *Inorg. Chem.* **1999**, *38*, 4585−4592.
(56) Cotton F. A.; Wilkinson, G. *Advanced Inorganic Chemistry*, 4th ed.; John Wiley and Sons: New York, 1980; pp 1017−1020.

Received for review May 28, 2004. Revised manuscript received November 9, 2004. Accepted November 29, 2004.

ES049201J